Model-Based Evaluation of Signal-to-Clutter Ratio for Landmine Detection Using Ground-Penetrating Radar

Giannakis, Iraklis; Giannopoulos, Antonios; Yarovoy, Alexander

Published in:
IEEE Transactions on Geoscience and Remote Sensing

DOI:
10.1109/TGRS.2016.2520298

Publication date:
2016

Document Version
Peer reviewed version

Model-Based Evaluation of Signal to Clutter Ratio for Landmine Detection Using Ground Penetrating Radar

Iraklis Giannakis, Antonios Giannopoulos, and Alexander Yarovoy [*†‡]

November 16, 2015

Abstract

A regression model is developed in order to estimate in real time the signal to clutter ratio (SCR) for landmine detection using ground penetrating radar (GPR). Artificial neural networks (ANN) are employed in order to express SCR with respect to the soil's properties, the depth of the target and the central frequency of the pulse. The SCR is

[†]Iraklis Giannakis and Alexander Yarovoy are with the Delft University of Technology, department of Microelectronics, group of Microwave Sensing, Signals and Systems MS^3, TU Delft, Faculty EEMCS (building 36), Mekelweg 4, 2628 CD Delft, Netherlands. (e-mail: I.Giannakis@tudelft.nl, A.Yarovoy@tudelft.nl).

[‡]Antonios Giannopoulos is with the Institute of Infrastructure and Environment, School of Engineering, The University of Edinburgh, Edinburgh EH9 3JL, U.K. (e-mail: A.Giannopoulos@ed.ac.uk).

synthetically evaluated for a wide range of diverse and **controlled** scenarios using the finite difference time-domain (FDTD) method. Fractals are used to describe the geometry of the soil's heterogeneities as well as the roughness of the surface. The dispersive dielectric properties of the soil are expressed with respect to traditionally used soil's parameters, namely, sand fraction, clay fraction, water fraction, bulk density and particle's density. Through this approach, a coherent and uniformly distributed training set is created. The overall performance of the resulting non-linear function is evaluated using scenarios which are not included in the training process. The calculated and the predicted SCR are in good agreement indicating the validity and the generalisation capabilities of the suggested framework.

Index Terms – ANN, clutter, FDTD, fractals, GPR, landmines, regression, SCR.

I Introduction

The term "Anti-Personnel (AP) landmine" includes a wide range of different explosive devices designed to maim or kill pedestrians [1], [2]. AP landmines are typically shallow-buried (no more than 10 cm) [1], [2] and can be found in a wide range of environments (urban environments, deserts, jungles and so on) [3]. Humanitarian demining tries to detect and disable AP and anti-vehicle landmines while balancing between efficiency and safety. Numerous approaches

from a diverse set of scientific fields have been proposed in an effort to assist humanitarian demining, from metal detector (MD) [4], [5] and electrical resistivity tomography (ERT) [6], [7] to trained rats [8], **artificial noses** [9] and acoustic methods [10]. In the same context, GPR has been shown to be a promising demining approach [11], [12] and a number of commercial GPR-based demining tools are now available for field operations [13], [14].

The main advantage of GPR is its ability to detect both metallic and non-metallic targets (in contrast to MD). Furthermore, GPR can provide an insight regarding the nature of the target (size, burial depth and so on). From the above, it is evident that GPR can potentially reduce the false alarms emerging from small metallic objects (bullets, wires, etc.) often encountered in battle-fields and industrialised areas. Combining the robustness of MD with the resolution of GPR results to a reliable and efficient detection-framework. The latter has been successfully applied in Cambodia and Afghanistan [15].

However, GPR's performance is limited due to the presence of electromagnetic losses and unwanted clutter. While soil attenuation is relatively well studied [11], estimation and prediction of soil-clutter remains mainly an open issue. In general, ground reflection constitutes the most dominant part of the clutter [16]. In addition, soil's heterogeneities can significantly contribute to the overall clutter especially in soils with highly heterogeneous moisture distribution [17], [18]. Regardless of its origin, unwanted clutter increases with frequency [12]. This has major effects to high-frequency applications such as

GPR for AP landmine detection. A proper estimation of the clutter for a particular operational scenario can potentially assist demining via selecting the optimised frequency-band (and correspondingly, proper GPR sensor) for a given set of soil properties [11].

Different processing approaches have been suggested in an effort to reduce clutter and to enhance the overall GPR's performance. An adapted ground removal technique is proposed by [19] in order to suppress the irregular clutter resulting from the rough surface. In the same context, an exponential-based approximation of the clutter is suggested by [20] which is subsequently subtracted from the original data. In [21] a review of the ground removal techniques is given emphasizing on high pass filter, moving average removal, adaptive scaled and shifted (ASaS) filter [22] and two-sided linear prediction. Principal components analysis (PCA) and singular value decomposition (SVD) [23] have also been proposed in order to eliminate high and low correlation features associated with the ground-bounce and the high frequency clutter respectively. Extensive research has also been conducted focusing on single A-traces [14]. In addition, Kalman filter, wavelet packet decomposition, matched filter deconvolution and symmetry filters are some of the methods (among others) proposed to improve landmine detection using GPR [24].

The aforementioned processing **algorithms** try to enhance the detectability of GPR by increasing the overall SCR. The latter is case sensitive and highly related to the environment, the probing waveform (operational band-

width) and the antenna unit [25], [26]. Due to that, evaluation of SCR, either via measurements or direct numerical simulations is a time consuming task. In the present study a regression model is developed which establishes the algebraic relationship of SCR to the soil's properties, the roughness of the surface, the depth of the landmine and the central frequency of the pulse.

The proposed model is based on a back-propagation ANN [27]. In order to fully resolve the complexity of the feature space, a large number of randomly chosen scenarios are employed during the training process. Subject to the training set, the weights of the ANN are tuned using a scaled complex-conjugate optimization method [28]. Subsequently, the performance of the resulting ANN is evaluated in scenarios which are not included in the training **step** (testing set). The predicted (using ANN) SCR and the testing set are in good agreement indicating that the suggested regression framework can sufficiently model the nature and the behaviour of SCR.

Synthetic data, evaluated using the FDTD method [29], [30] are employed in the present paper for both training and testing purposes. Due to computational constrains [26], 2D geometries are considered. If computational resources are available, the proposed method can be extended to 3D geometries providing a platform for comparing different antenna units in a variety of environments. **Modelling commercial systems is not a straightforward task since information is not trivially available due to confidentiality issues. Nonetheless, when adequate information is available, commercial antennas can be accurately modelled using**

numerical solvers like FDTD [31]. In addition, recent advantages to gprMax [32], [33] (www.gprmax.com) make it possible for the manufacturers to provide electromagnetic models of their antennas without revealing any information to the users, thus respecting the confidentiality constrains [34].

Soil's heterogeneities and rough surfaces are simulated using fractal correlated noise. The latter, it has been proven that can sufficiently represent both the spatial correlation of the soil's properties [35], [36] as well as the roughness of the surface [37], [38]. Regarding the dielectric properties of the soil, a semi-empirical model [39], [40] is used which expresses soil's dispersive dielectric properties with respect to its sand fraction, clay fraction, water volumetric fraction, particle's density and bulk density [39], [40]. The target of interest is represented by the AP landmine PMA-1. Lastly, a Gaussian-modulated sinusoidal pulse (representing the one's typically employed in GPR) is implemented to FDTD as an impressed current source.

The rest of the paper is organized as follows. Details over SCR evaluation using FDTD are presented in Section II. Regression modelling using ANN and verification of the developed model are presented in Section III. A number of representative case studies are demonstrated in Section IV. Finally, the conclusions are drawn in Section V.

II SCR Evaluation Using FDTD

II.1 Dielectric properties of soil

Soils are complex media which are primarily consisted of sand, clay, water and air. **Based on these elements, soils can be classified accordingly e.g. dry sand, saturated clay and so on. Soils can be further categorised based on their chemical composition and their organic fraction [41]. Nonetheless, classifying soils based on their particle's size (sand, clay) is proven to be a valid simplification for predicting soil's dielectric properties [39].**

The size of the soil's particles, as well as the volume of the pores are orders of magnitude smaller than the typical wavelengths employed in GPR. Due to that, the bulk dielectric properties of the soil can be accurately expressed with respect to the dielectric properties of its elements [42], [43].

In the present study we use the semi-empirical model initially suggested by [39] for the frequency range of 1.4-18 GHz. The main advantage of the semi-empirical model is that it evaluates the frequency-dependent electrical permittivity of the soil based on its most dominant elements (sand, clay, water and air). The semi-empirical model was initially proposed for high frequency applications [35]. Later on, a modification was proposed by [40], [44] in order to expand the semi-empirical model to lower frequencies (0.3-1.3 GHz). In the present study the adaptation proposed by [40], [44] is employed since its range of validity is closer to the frequency range used for

AP landmine detection.

The semi-empirical model [39], [40], [44] is described by the equations (1)-(9), where $\epsilon = \epsilon' + j\epsilon''$, j is the imaginary unit $\left(j = \sqrt{-1}\right)$, f_w is the water volumetric fraction, ρ_s is the **mean** particle's density (g/cm^3), ρ_b is the bulk density of the soil (g/cm^3), ϵ_s is the relative permittivity of the sand particles, $a = 0.65$ is an experimentally derived constant, S is the sand mass fraction and C is the clay mass fraction ($0 \leq \{S, C\} \leq 1$ and $S + C = 1$). The relative permittivity of the water is $\epsilon_w = \epsilon'_w + j\epsilon''_w$ (7) where $t_{0,w} = 9.23$ ps is the relaxation time, $\epsilon_{w,0} = 80.1$ is the relative permittivity for zero frequency and $\epsilon_{w,\infty} = 4.9$ is the relative permittivity for infinity frequency [40]. The term σ_f is linearly related to the conductivity σ [25], [26].

$$\epsilon'_{(1.4-18\ GHz)} = \left(1 + \frac{\rho_b}{\rho_s}(\epsilon_s^a - 1) + f_w^{\beta'}\epsilon_w'^a - f_w\right)^{1/a} \tag{1}$$

$$\epsilon'_{(0.3-1.3\ GHz)} = 1.15\epsilon'_{(1.4-18\ GHz)} - 0.68 \tag{2}$$

$$\epsilon'' = -f_w^{\frac{\beta''}{a}}\left(\epsilon''_w + \frac{\sigma_f}{\omega\epsilon_0}\frac{(\rho_s - \rho_b)}{\rho_s f_w}\right) \tag{3}$$

$$\epsilon_s = (1.01 + 0.44\rho_s)^2 - 0.062 \tag{4}$$

$$\beta' = 1.2748 - 0.519S - 0.152C \tag{5}$$

$$\beta'' = 1.33797 - 0.603S - 0.166C \tag{6}$$

$$\epsilon_w = \epsilon_{w,\infty} + \frac{\epsilon_{w,0} - \epsilon_{w,\infty}}{1 + j\omega t_{0,w}} \tag{7}$$

$$\sigma_{f(1.4-18\ GHz)} = -1.645 + 1.939\rho_b - 2.25622\ S + 1.594C \tag{8}$$

$$\sigma_{f(0.3-1.3\ GHz)} = 0.0467 + 0.2204\rho_b - 0.411\ S + 0.6614C \tag{9}$$

The semi-empirical model described in (1)-(9) can not be directly implemented to FDTD [25], [26]. Similar to [25] and [26], Debye expansions are used in an effort to approximate the semi-empirical model (for the frequency range of interest) using functions which are compatible with FDTD. As it is shown in [25], [26], a single Debye pole plus a conductive term can sufficiently approximate the semi-empirical model for frequencies below 5 GHz.

Implementing dispersive media into FDTD increases the overall computational requirements [29]. **Nonetheless, for high frequency problems (like GPR for AP landmine detection), implementing the dipolar losses of soils is highly important since the latter can substantially decrease the amplitude of the received A-Scan and distort its shape. Fig. 1 illustrates the resulting scattering field from a low dielectric target (AP landmine PMA-1) buried at 10 cm depth in a homogeneous saturated sand. It is evident that both the amplitude and the spectral shape of the reflected wave is affected due to the presence of dipolar relaxation mechanisms within the soil. Dipolar losses can have a significant effect on high frequencies and should neither be neglected nor simply defined.**

II.2 Soil's geometry

With the term "soil's geometry" we define the spatial distribution of the soil's properties and the roughness of the surface. Soil's geometry is stochastic [35], [38] *i.e.* it can be described by a random process which can be statistically defined but not precisely predicted. Fractal correlated noise is a well known stochastic procedure which is considered as an attractive approach for simulating soil's geometry [35], [38]. The self-similarity imposed in fractals is the reason why fractal correlated noise can simulate soil with sufficient detail [38]. Self-similarity is frequently encountered in nature and it is the reason why on geoscience-related photos everyday objects are necessary for **visual** purposes.

Furthermore, in [37] and [38], experimental evidences are given which support the premise that earth's topography can be sufficiently approximated using fractals. Apart from topography, the spatial distribution of various environmental data also obey fractals laws [35], [36]. In particular, regarding the distribution of water within the soil, solid evidences are given in [45] which support the premise that soil's pores (both the size and the network structure) obeys a power law. It is obvious that soil's pores and water volumetric fraction are directly related. It is also known that power law has a linear relationship with fractals [46]. From the above, it is concluded that the spatial variation of the water volumetric fraction within the soils can be effectively described using fractals.

Fractal correlated noise for n dimensions can be generated through

$$F\left(x_1, x_2 ... x_n\right) = \mathcal{F}^{-1}\left(R\left(k_1, k_2, ... k_n\right) \cdot \left(\sum_{i=1}^{n} k_i^2\right)^{-\frac{\beta}{2}}\right) \tag{10}$$

where F is the resulting fractal correlated noise, x_i is the ith dimension, R is the Fourier transform of a nth-dimensional Gaussian noise, k_i is the ith dimension in the wavenumber domain, β is a linearly-related term to the fractal dimension (known as Hurst exponent) [46] and $\mathcal{F}^{-1}$ denotes the inverse Fourier transform symbol. **As β increases, the correlation length of F increases as well [38]. This indicates that β is inversely proportional to the spatial derivatives and the roughness of F.**

Using (10) and rescaling according to the desired minimum and maximum water volumetric fraction, different soils with different spatial variations of water volumetric fraction (different β) can be generated. In the same context, different surfaces can be modelled subject to a given fractal dimension and a pre-defined **minimum and maximum amplitude**. Application of fractal correlated noise to modelling surface clutter is coherently described in [49]. Fig. 2 illustrates a representative sample of the generated models using fractal correlated noise.

II.3 Target Model

The AP landmine PMA-1 is chosen to represent a generic low dielectric target. The modelled landmine is based (see Fig. 2) on the model described

in [25], [26]. PMA-1 can be found both with and without metal fuse. In the present paper no metallic parts are incorporated in the modelled PMA-1 in an effort to create a more challenging platform with respect to SCR estimation.

II.4 Impressed Current Sources

Impressed current sources, also known as soft sources, are chosen to excite the FDTD grid. Soft sources, in contrast with hard sources, do not interact with the propagating field [29]. This is particularly attractive for near field applications (like GPR for landmine detection) and **this is** the main reason why soft sources are considered in the present paper.

The shape of the excitation pulse is a Gaussian modulated sinusoidal function [50]

$$J(t) = \exp\left(-\frac{(2\pi \cdot t \cdot bw \cdot fc)^2}{11.0524}\right) \cos\left(2\pi \cdot fc \cdot t\right) \tag{11}$$

where t is time (s), fc is the central frequency of the pulse (Hz) and bw is a non-unit constant which denotes the fractional bandwidth of (11). Fig. 3 illustrates a set of Gaussian modulated sinusoidal pulses using the same fractional bandwidth ($bw = 0.9$) for different central frequencies (fc).

II.5 FDTD simulations

Without loss of generality, the received A-Scan over an AP landmine can be expressed as

$$G = G_q + G_c + G_s \tag{12}$$

where G is the raw A-Scan, G_q is the **incident** field, G_c is the clutter and G_s is the signal *i.e.* the resulting scattering field due to the presence of PMA-1.

Ground-removal techniques are typically applied to the raw data in an effort to suppress the direct wave and the ground reflection. These techniques [19]-[22] would ideally work in the presence of a homogeneous medium subject to a flat surface. Any deviation from these ideal conditions reduces the effectiveness of ground-removal methods. In that context, we define as **incident** field G_q the field which would occur if the soil was homogeneous with flat surface. The clutter G_c is defined as the difference of the total field in the absence of the landmine minus the **incident** field (G_q). Through that, we indirectly implement a generic ground removal before estimating the clutter. Thus, the clutter neither includes the direct wave nor the reflection of an average surface. Only the deviations from the ideal scenario (homogeneous soil with flat surface) are considered as scattering sources. Knowing G, G_q and G_c, the signal G_s can be trivially calculated from (12).

The FDTD method [29], [30] is chosen for the evaluation of (12). The spatial discretization step of the FDTD is uniform along the grid with $\Delta x = \Delta z = 1$ mm. The time discretization equals 0.99 times the Courant limit

[29], [30]. The Debye relaxation mechanisms of the soil are implemented using the current density (CD) method [47]. Regarding the absorbing boundary conditions (ABC), a time-synchronised perfectly matched layer (PML) [48] is applied with ten-layers thickness.

In an effort to create a coherent and equally distributed training set, a large number of randomly selected scenarios are created and their corresponding SCR is subsequently evaluated. Following this approach, results to a uniformly distributed training set which includes a wide range of scenarios varying from dry to saturated environments, homogeneous to highly complex soils, flat to rough surfaces, shallow to deep buried targets and so on (see Fig. 2). This is critical in order to fully and equally represent the feature space without being biased to specific cases while neglecting others.

A detailed step-by-step description of the procedure applied to generate the training set is outlined below:

- The excitation pulse is a Gaussian-modulated sinusoidal function (11) with fractional bandwidth equals to $bw = 0.9$. The central frequency of the pulse f_c is randomly selected using a uniform distribution varying from 0.9 to 3 GHz (typical frequency range used for AP landmine detection). **The height of the source is assumed constant at 5 cm above the average soil's surface. This is a valid assumption since the majority of the commercial systems associated with demining are ground coupled antennas which operate in a close proximity to the ground [14], [15], [24].**

- The minimum m and the maximum M value of the water fraction are randomly selected based on a uniform distribution which varies from 0 to 0.3.

- The sand fraction S is randomly selected based on a uniform distribution varying from 0 to 1. Subsequently the clay fraction is calculated by $C = 1 - S$. The sand and the clay fractions are assumed uniform along the grid.

- The water volumetric fraction of the soil has a stochastic spatial variation which is described by (10). The value of β_w is randomly selected using a uniform distribution varying from 0 to 3.5.

- **The maximum absolute deviation of the topography (T) is defined as**

$$T = \max_{x \in \mathcal{R}} ||Top\,(x) - \text{mean}\,(Top\,(x))\,|| \tag{13}$$

  where $Top(x)$ is the topography with respect to x. The maximum absolute deviation of the surface is chosen using a uniform distribution varying from 0 to 30 mm.

- The roughness of the soil's surface is described by (10). The value of β_T is randomly chosen using a uniform distribution varying from 2 to 4.5.

- Based on the parameters given in the previous steps and using (10), a stochastic soil is generated with a fractal variation of water fraction

subject to a fractal rough surface. The clay as well as the sand fraction are assumed uniform along the soil and their values are randomly chosen. Bulk and particle's density are also considered uniform and their values are set to $\rho_b = 1.5$ gr/cm^3 and $\rho_s = 2.66$ gr/cm^3 (typical values for soils).

- Using (1)-(9), the dielectric properties of the soil are calculated and subsequently are approximated using a Debye function plus a conductive term [25]. The resulting distribution of the dielectric properties is used as input to FDTD. The output trace equals with $G_q + G_c$ (**incident field** plus clutter).

- Subsequently, a half-space model (homogeneous soil with flat surface) is generated in order to calculate the **incident** field G_q (using FDTD). The water volumetric fraction of the aforementioned model is uniform and equal to the mean value of the stochastic model (described at the previous steps). Knowing G_q and $G_q + G_c$ (from the previous step), the clutter G_c can be calculated in a straightforward manner.

- The AP landmine PMA-1 is added to the stochastic soil. Its depth D is randomly selected using a uniform distribution varying from 0 to 100 mm (typical depths for AP landmines). Using FDTD, the raw A-Scan G is calculated. Knowing G, G_q and G_c (from the previous steps), the signal G_s can be trivially evaluated from (12).

- Lastly, the SCR is calculated through

$$SCR = 20 \cdot \log_{10} \left(\frac{\max\{||G_s||\}}{\max\{||G_c||\}} \right). \tag{14}$$

The above scheme is repeated until the feature space is adequately resolved. For the present regression model, it is proven that ten thousands data can sufficiently represent the feature space of the problem (more details are provided in **Section** III).

Fig. 4 illustrates the probability density function (PDF) of the synthetically evaluated SCR using the procedure **previously** explained. A Gaussian distribution can sufficiently represents the PDF of SCR. The mean value and the standard deviation of SCR equal to -5.9 dB and 13.74 dB respectively. Notice that neither gain nor any kind of processing (apart from the generic ground removal) are applied to the data prior to SCR estimation.

III Regression Modelling of SCR using ANN

Regression modelling (or regression analysis) tries to estimate the relationship (if any) between given inputs and their corresponding outputs [27]. In the present study, regression modelling using ANN is applied in order to unravel the underlying relationship between given inputs and SCR. In particular, the inputs are:

- Sand fraction (S)

- Depth of the landmine (D)
- Minimum water volumetric fraction (m)
- Maximum water volumetric fraction (M)
- Spatial statistics of water volumetric fraction (β_w)
- Maximum absolute deviation of the surface (T)
- Spatial statistics of soil's surface **(roughness)** (β_T)
- Central frequency of the pulse (f_c)

Millions of scenarios need to be examined in order to fully explore the feature space defined by the aforementioned inputs. Moreover, the stochastic properties of the soil results to a stochastic variation of SCR *i.e.* different SCR occurs for the same inputs. Thus, the average SCR for a specific scenario is to be predicted. This means that a sufficient number of models must be simulated for each unique set of inputs. From the above, it is evident that a brute-force approach using pre-calculated data is not a practical method for predicting and estimating SCR for a wide range of environments.

Regression modelling using ANN has the potential to find the underlying relationship between the inputs and SCR using a limited number of data. To do so, the training database must be representative of the feature space. Using the approach explained in Section II.5, a sufficiently large (ten thousands data) and equally distributed training set is created.

The synthetically generated training set is subsequently used to train a feedforward ANN with two hidden layers. The number of neurones of the first and the second layer are ten and five neurones, respectively. The activation functions (AF) are all sigmoids apart from the output layer which is linear. Fig. 5 illustrates the structure of the ANN chosen for the present study. A trial and error procedure is used to adjust the neural structure in an effort to increase the accuracy without using unnecessary large number of neurones and hidden layers (which would result to over-fitting [27]). A scaled complex-conjugate optimization method [28] is applied in order to tune the weights of ANN such as the mean squared error between the predicted and the actual SCR to be minimised. In order to avoid over-fitting and to increase the generalisation capabilities of ANN (as it is stated earlier) a simple neural structure is selected. In addition, the generalisation capabilities of the resulting ANN are further strengthened by using 10% of the data for cross-validation purposes during the training process [27].

The validity and the generalisation capabilities of the suggested ANN are tested on unknown cases that are not included in the training set. A wide range of randomly selected scenarios are used as a testing platform. Due to the stochastic nature of the soil, the statistical properties and not the actual spatial variation for both water fraction and surface elevation are given as inputs. In that context, fifteen realisations take place for each testing scenario in order to evaluate the mean value of the resulting SCR. The calculated (using FDTD) and the predicted SCR (using ANN) are in

good agreement (see Fig. 6) indicating the generalisation capabilities of the proposed regression model. Fig. 7 illustrates the PDF of the error between the calculated and the predicted SCR. The mean value is -0.07 dB and the standard deviation equals 1.8 dB.

As it is stated earlier, ten thousands data are used for both training and validation purposes (90% for training and 10% for cross-validation). This number is chosen based on the observation that further increase of the training set does not substantially affect the performance of the proposed regression model.

Fig. 8 illustrates the mean squared error using different percentages of the original database. Since the training process is an iterative technique, the resulting ANN are related to the initial weights and biases chosen prior to the optimisation. In that context, the mean squared error illustrated in Fig. 8 is the average of twenty different ANN resulting using different initial weights and biases. From Fig. 8 it is apparent that both the average and the standard deviation of the mean squared error start converging to a minimum when 90 % of the original database are employed for training and 10 % for cross-validation purposes.

IV Numerical Study

The proposed regression model is used in order to evaluate (in real time) SCR for three representative case studies. The present examples are chosen such as to emphasize on the effects of the inputs to the overall performance of GPR.

In the first scenario, a homogeneous saturated soil is examined with $m = 0.1$, $M = 0.101$, $C = 0.5$, $\beta_T = 3$, $\beta_w = 1$, $f_c = 0.9 - 3$ GHz and $D = 0 - 60$ mm. Three different **maximum absolute deviations** are chosen ($T = 0$ mm, $T = 2$ mm and $T = 20$ mm) in order to emphasize on the relationship between T and SCR. From Fig. 9 it is evident that rough surfaces decrease the overall performance of GPR. The effects of rough surface are more dominant when higher frequencies are employed. The latter, due to their small wavelengths can sufficiently resolve the roughness of the surface which leads to the decrease of SCR. From the above (and as it is clearly shown in Fig. 9), it is concluded that lower frequencies are more suitable for large values of T.

Regarding the relationship between D (landmine's depth) and SCR, larger D results to lower signal thus lower SCR. In addition, the dipolar relaxation mechanisms within the soil (see **Section** II), rapidly absorb high frequencies when water is present. Due to that, the optimal central frequency (which maximizes SCR for a given scenario) is decreased as the burial depth increases (see Fig. 9).

In the second example we examine how the distribution of water within the soil can affect the overall SCR. A flat-surface is chosen in order to emphasize on the effects of soil's heterogeneities. The inputs of the model are $m = 0.05$, $M = 0.2$, $C = 0.5$, $\beta_T = 3$, $T = 0$, $f_c = 0.9-3$ GHz and $D = 0-60$ mm. **Here, β_T is irrelevant since $T = 0$. The value $\beta_T = 3$ is chosen arbitarilly, different values of β_T result to the same outputs when** $T = 0$. Three different water distributions are tested A) $\beta_w = 0$, B) $\beta_w = 0.8$ and C) $\beta_w = 1.4$. As β_w increases, the correlation length of the water fraction increases as well. From Fig. 10, it is evident that the correlation length of the water's fraction is inversely proportional to SCR. Similar to the previous example, the effects of β_w are more dominant when high frequencies are used. This due to the fact that high frequencies (small wavelengths) can sufficiently resolve small targets such as soil's heterogeneities. This increases the unwanted clutter emerging from soil's spatial heterogeneities and furthermore decreases the overall performance of GPR.

The last example focuses on the effects of surface's correlation length (implicitly described by β_T) to the performance of GPR. A homogeneous saturated soil is examined in order to focus on the underlying relationship between β_T and SCR. The inputs of the model are $m = 0.10$, $M = 0.101$, $C = 0.5$, $\beta_w = 1$. $f_c = 1.5$ GHz, $D = 35$ mm, $T = 2 - 10$ and $\beta_T = 2 - 4.5$. Fig. 11 clearly illustrates that both the correlation length of the soil's surface and the maximum absolute deviation of the surface reduce SCR. In particular, for the same maximum absolute deviation, smooth surfaces

(large β_T) result to lower SCR compared to surfaces with small correlation length (small β_T). This is due to the generic ground removal **applied to the training set (see Section II.5)** which assumes a homogeneous soil with flat surface. Any variation from the aforementioned assumption is treated as clutter. Thus, clutter subtraction in the case of **smooth surfaces**, results to large segments which act as large targets easy to be resolved due to their size.

To further support the results illustrated in Fig. 11, three models are synthetically modelled using different β_T (see Fig. 12). Average removal and SVD ($\lambda_i,\ i < 3$, where λ_i is the ith eigenvalue of the B-Scan) are applied in an effort to suppress the ground reflection and increase the overall SCR. Both of the employed techniques try to remove the spatially correlated features associated with the ground reflection and the direct wave. Thus, they resemble the generic ground removal applied prior to the evaluation of SCR (see Section II.5). From Fig. 12 it is evident that increasing β_T reduces the effectiveness of ground removal techniques as predicted by the proposed regression model (see Fig. 11).

V Conclusions

A regression model using ANN is developed in order to model and predict (in real time) SCR for a wide range of diverse scenarios. Resolving the present feature space requires an equally distributed and adequately large

training set. The latter is synthetically generated using FDTD. Fractal correlated noise is chosen for modelling both the soil's heterogeneities and the surface of the soil. The dielectric properties of the soil are expressed using a semi-empirical model which (for implementation purposes) is approximated by a conductive term plus a Debye pole. Via numerical experiments it is shown, that the proposed framework can unravel the underlying relationship between medium properties and SCR using a limited number of training data. The generalisation capabilities of the suggested regression model are demonstrated on a large number of randomly selected scenarios which were not included in the training process. If adequate computational resources are available, the proposed framework can be expanded to 3D geometries providing a real-time platform for comparing the performance of different GPR units to a wide range of diverse scenarios. In addition, the suggested approach can be trivially modified to include other classes of targets, *e.g.* cables, pipes, air voids and so on.

Acknowledgement

The present paper has been prepared in the frame of the FP7 project D-BOX (www.d-boxproject.eu) under the grant agreement no. 284996.

References

[1] M. A. Cameron, R. J. Lawson and B. W. Tomlin, *To walk without fear: The global movement to ban landmines*, Oxford University Press, USA, First Edition, 1998.

[2] K. Bjork, *Riding the world of landmines: The governance of mine action*, Brown Walker Press, USA, First Edition, 2012.

[3] D. J. Daniels, "A review of GPR for landmine detection," *Int. J. of Sensing and Imaging*, vol. 7, no. 3, pp. 90-123, Dec. 2006.

[4] M. Acheroy, "Mine action: status of sensor technology for close-in and remote detection of anti-personnel mines," *Near Surface Geophysics*, vol. 5, pp. 43-55, Feb. 2007.

[5] B. Claudio, G. Bertrand, G. Frederic, P. Pierre-Yves and C. Olivier, "Ground penetrating radar and imaging metal detector for antipersonnel detection," *J. of Applied Geophysics*, vol. 40, pp. 59-71, Oct. 1998.

[6] P. Church, J. E. McFee, S. Gagnon and P. Wort, "Electrical impedance tomographic imaging of buried landmines," *IEEE Trans. Geosci. Remote Sens.*, vol. 44, no. 9, pp. 2407-2420, Sept. 2006.

[7] M. Metwaly, "Detection of metallic and plastic landmines using GPR and 2-D resistivity techniques," *Nat. Hazards Earth Syst. Sci.,* vol. 7, pp. 755-763, Dec. 2007.

[8] APOPO 2006, a Belgian research organisation that was initiated in response to the global landmine problem. http://www.apopo.org/ , 1 Sept. 2015.

[9] M. Acheroy, "Mine-action: status of sensor technology for close-in and remote detection of antipersonnel mines," in *Proc. 3rd Int. Workshop on Advanced Ground Penetrating Radar,* pp. 3-13, May 2005.

[10] C. T. Schroder and W. R. Scott, "A finite-difference model to study the elastic-wave interactions with buried landmines," *IEEE Trans. Geosci. Remote Sens.*, vol. 38, no. 4, pp. 1505-1512, Jul. 2000.

[11] A. Yarovoy, "Landmine and UXO Detection and Classification," in *Ground Penetrating Radar Theory and Applications*, Oxford, Elsevier, 2008.

[12] D. J. Daniels, *Ground Penetrating Radar*, London, IEE Radar, Sonar, Navigations and Avionics Series 15, The institution of Engineering and Technology, 2nd Edition, 2004.

[13] A. Yarovoy and M. Sato, "Mine detection," in *Subsurface Sensing*, New Jersey, John Wiley & Sons, 2011.

[14] D. J. Daniels, "A review of landmine detection using GPR," in *Proc. EuRAD*, Amsterdam, pp. 280-283, 2008.

[15] D. J. Daniels, J. Braunstein and M. Nevard, "Using MINEHOUND in Cambodia and Afghanistan," *The J. of ERW and Mine Action*, issue 18.2, 2014.

[16] D. Potin, E. Duflos and P. Vanheeghe, "Landmines ground-penetrating radar signal enhancement by digital filtering," *IEEE Trans. Geosci. Remote Sens.*, vol. 44, no. 9, pp. 2393-2406, 2006.

[17] K. Takahashi, J. Igel and H. Preetz, "Modeling of GPR clutter caused by soil heterogeneity," *Int. J. of Antennas and Propag.*, vol. 2012, Article ID 643430, 7 pages, 2012.

[18] K. Takahashi, J. Igel, H. Preetz and M. Sato, "Influence of heterogeneous soils and clutter in the performance of ground-penetrating radar for landmine detection," *IEEE Trans. Geosci. Remote Sens.*, vol. 52, no. 6, pp. 3464-3472, 2014.

[19] H. Brunzell, "Detection of shallowly buried objects using impulse radar," *IEEE Trans. Geosci. Remote Sens.*, vol. 37, no. 2, pp. 875-886, Mar. 1999.

[20] A. Merwe and I. Gupta, "A novel signal processing technique for clutter reduction in GPR measurements of small, shallow landmines," *IEEE Trans. Geosci. Remote Sens.*, vol. 38, no. 6, pp. 2627-2637, Nov. 2000.

[21] A. M. Mayordomo and A. Yarovoy, "Optimal background subtraction in GPR for humanitarian demining," in *Proc. EuRadar*, Amsterdam, pp. 48-51, 2008.

[22] R. Wu, A. Clement, J. Li, E. G. Larsson, M. Bradley, J. Habersat and G. Maksymonko, "Adaptive ground bounce removal," *IEEE Electronic Lett.*, vol. 37, no. 20, pp. 1250-1252, Sep. 2001.

[23] K. Park, S. Park, K. Kim and K. Hee Ko, "Multi-feature based detection of landmines using ground penetrating radar," *Progress In Electromagnetics Research*, vol. 134, pp. 455-474, 2013.

[24] G. T. Tesfamariam, *Signal Processing Techniques for Landmine Detection Using Impulse Ground Penetrating Radar*, PhD thesis submitted at Elektotechnik ind Informationstechnik der Technischen Universitat Darmstadt, 2013.

[25] I. Giannakis, A. Giannopoulos and N. Davidson, "Realistic modelling of ground penetrating radar for landmine detection using FDTD," in *Proc. Inter. Conf. on Ground Penetrating Radar (GPR)*, Brussels, pp. 983-989, 2014.

[26] I. Giannakis, A. Giannopoulos and C. Warren, "A realistic FDTD numerical modelling framework of ground penetrating radar for landmine detection," *IEEE J. Sel. Topics Appl. Earth Observ. in Remote Sens.*, vol. PP, no. 99, pp. 1-15, 2015.

[27] S. Haykin, *Neural Networks and Learning Machines*, New Jersey, Pearson, 3rd edition, 2008.

[28] M. F. Moller, "Scaled conjugate gradient algorithm for fast supervised learning," *Neural Networks*, vol. 6, pp. 525-533, 1993.

[29] A. Taflove and S. C. Hagness, *Computational Electrodynamics, the Finite-Difference Time-Domain Method,*, Norwood, MA: Artech House, 2nd edition, 2000.

[30] K. S. Kunz and R. J. Luebbers, *The Finite-Difference Time-Domain Method for Electromagnetics,* Boca Raton, FL: CRC Press, 1993.

[31] C. Warren and A. Giannopoulos, "Creating finite-difference time-domain models of commercial ground-penetrating radar antennas using Taguchi's optimisation method," *Geophysics*, vol. 76, no. 2, pp. G37-G47, Apr. 2011.

[32] A. Giannopoulos, "Modelling ground penetrating radar by gprMax," *Constructions and Buildings Materials*, vol. 19, pp. 755-762, 2005.

[33] C. Warren, A. Giannopoulos and I. Giannakis, "An advanced GPR modelling framework -the next generation of gprMax," In *Proc. 8th Int. Workshop in Advanced Ground Penetrating Radar.* pp. 1-4, 2015.

[34] C. Warren, A. Giannopoulos, N. Diamanti and P. Annan, "An extension module to embed commercially sensitive antenna models in gprMax," in *Proc. 8th Int. Workshop in Advanced Ground Penetrating Radar (IWAGPR),* pp. 1-3, 2015.

[35] D. Hillel, *Environmental Soil Physics*, San diego, Academic Press, 1980.

[36] P. A. Burrough, "Fractal dimensions of landscapes and other environmental data," *Nature*, vol. 294, pp. 240-242, 1981.

[37] D. L. Turcotte, "A fractal interpretation of topography and geoid spectra on the Earth, Moon, Venus and Mars," *J. Geophys. Res.*, vol. 92, no. B4, pp. E597- E601, Mar. 1987.

[38] D. L.Turcotte, *Fractals and chaos in geology and geophysics*, Cambridge, The Press Syndicate of the University of Cambridge, 1992.

[39] M. C. Dobson, F. T. Ulaby, M. T. Hallikainen and M. A. El-Rayes, "Microwave dielectric behavior of wet soil, Part II: Dielectric mixing models," *IEEE Trans. Geosci. Remote Sens.,* vol. GRS-23, pp. 35-46, Jan. 1985.

[40] N. R. Peplinski, F. T. Ulaby and M. C. Dobson, "Dielectric properties of soils in the 0.3-1.3 GHz range," *IEEE Trans. Geosci. Remote Sens.,* vol. 33, no. 3, pp. 803-807, May 1995.

[41] J. M. Carcione, *Wave propagation in anisotropic, anelastic, porous and electromagnetic media*, Elsevier, 3nd edition, 2015.

[42] R. J. Birchak, G. C. Gardner, E. J. Hipp and M. J. Victor, "High dielectric constant microwave probes for sensing soil moisture," in *Proc. of the IEEE*, vol. 62, no. 1, pp 93-98, 1974.

[43] M. A. Shutko and E. M. Reutov, "Mixture formulas applied in estimation of dielectric and radiative characteristics of soils and grounds at microwave frequencies," *IEEE Trans. Geosci. Remote Sens.*, vol. GE-20, no. 1, pp. 29-32, 1982.

[44] N. R. Peplinski, F. T. Ulaby and M. C. Dobson, "Corrections to dielectric properties of soils in the 0.3-1.3-GHz range," *IEEE Trans. Geosci. Remote Sens.,* vol. 33, no. 6, pp. 1340, Nov. 1995.

[45] S. Longsdom, M. Berli and R. Horn, *Quantifying and Modeling Soil Structure Dynamics*, Madison, Soil Science Society of America, 2013.

[46] T. Higuchi, "Relationship between the fractal dimension and the power law index for a time series: a numerical investigation," *Physica D*, vol. 46, pp. 254-264, 1990.

[47] I. Giannakis and A. Giannopoulos,"A novel piecewise linear recursive convolution approach for dispersive media using the finite-difference time-domain method," *IEEE Trans. Antennas Propag.*, vol. 62, no. 5, pp. 2669-2678, May 2014.

[48] I. Giannakis and A. Giannopoulos, "Time-synchronised convolutional perfectly matched layer for improved absorbing performance in FDTD," *IEEE Antennas and Wirele. Propag. Lett.*, vol. 14, pp. 690-693, 2015.

[49] A. Yarovoy, C. N. Vazouras, J. G. Fikioris and L. P. Lightart, "Numerical simulations of the scattered field near a statistically rough air-ground

interface," *IEEE Trans. Antennas Propag.*, vol. 52, no. 3, pp. 780-789, Mar. 2004.

[50] Z. G. Fan, L. X. Ran and J. A. Kong, "Source pulse optimisation for UWB radio systems," *J. of Electromagnetic Waves and Applications*, vol. 20, no. 11, pp. 1535-1550, 2006.

List of Figures

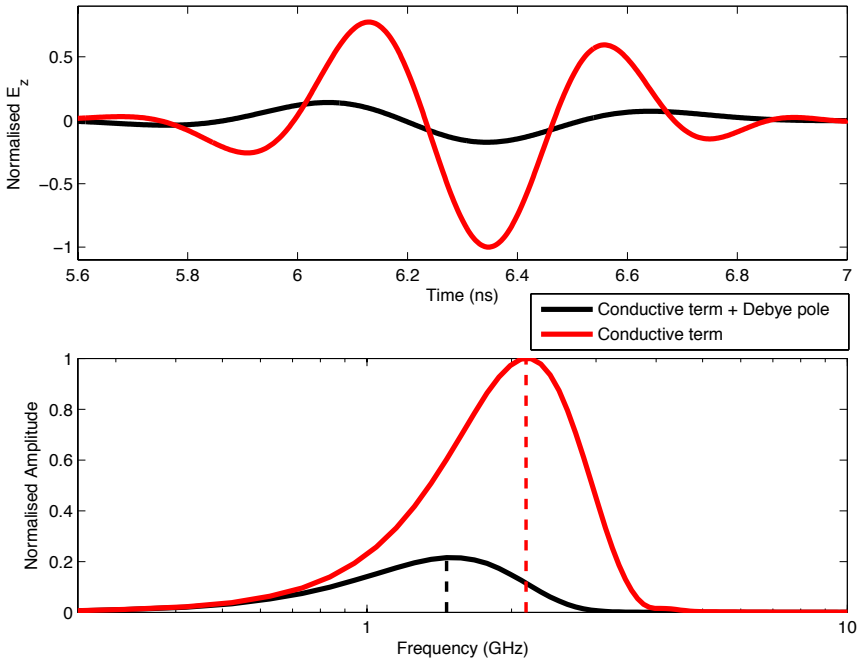

Figure 1: Scattering field from PMA-1 with and without dipolar losses. The AP landmine is buried in a homogeneous saturated sand with $S = 1$, $C = 0$, $\rho_b = 1.5$ gr/cm^3, $\rho_s = 2.66$ gr/cm^3 and $f_w = 0.3$. The depth of the landmine is 10 cm. The surface of the soil is flat and the central frequency of the pulse is equal to 2 GHz. The dipolar losses incorporated into the Debye pole can substantially decrease both the amplitude and the central frequency of the scattering field.

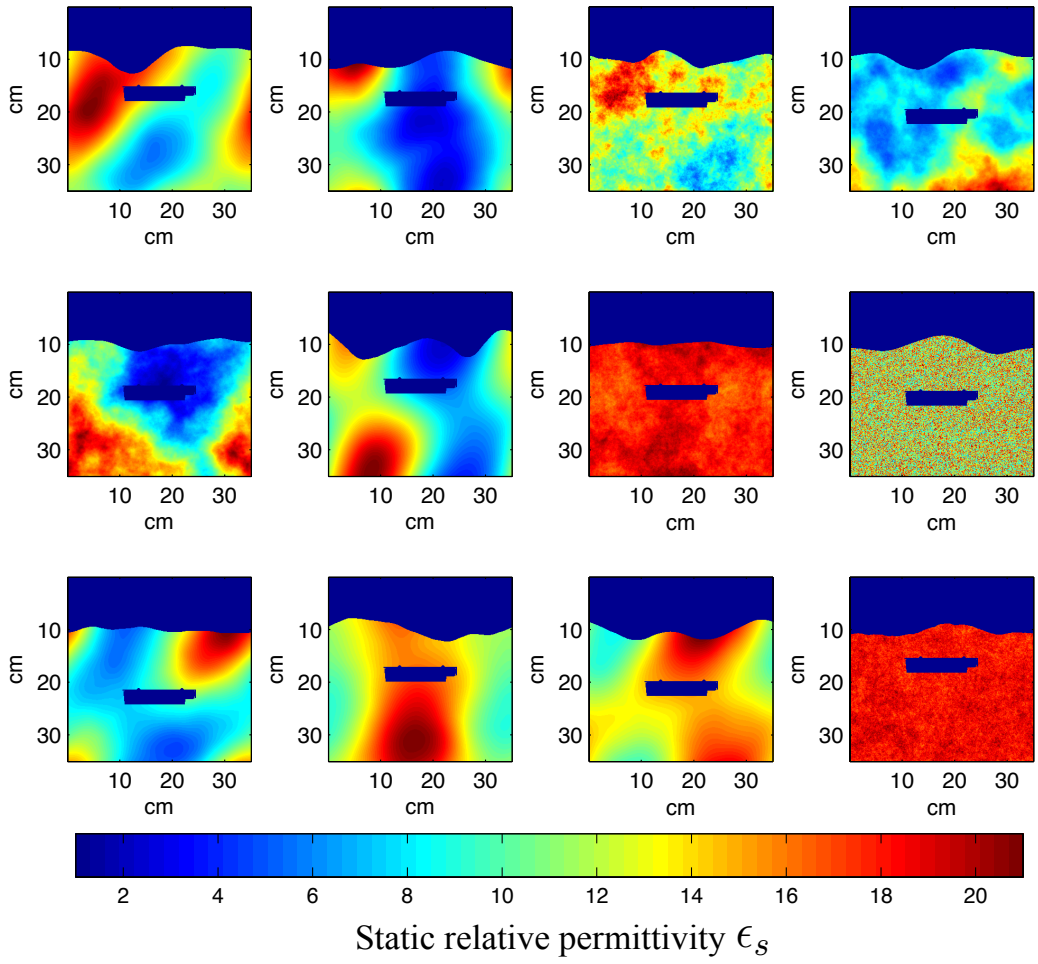

Figure 2: A representative sample of the models used to train the suggested regression framework.

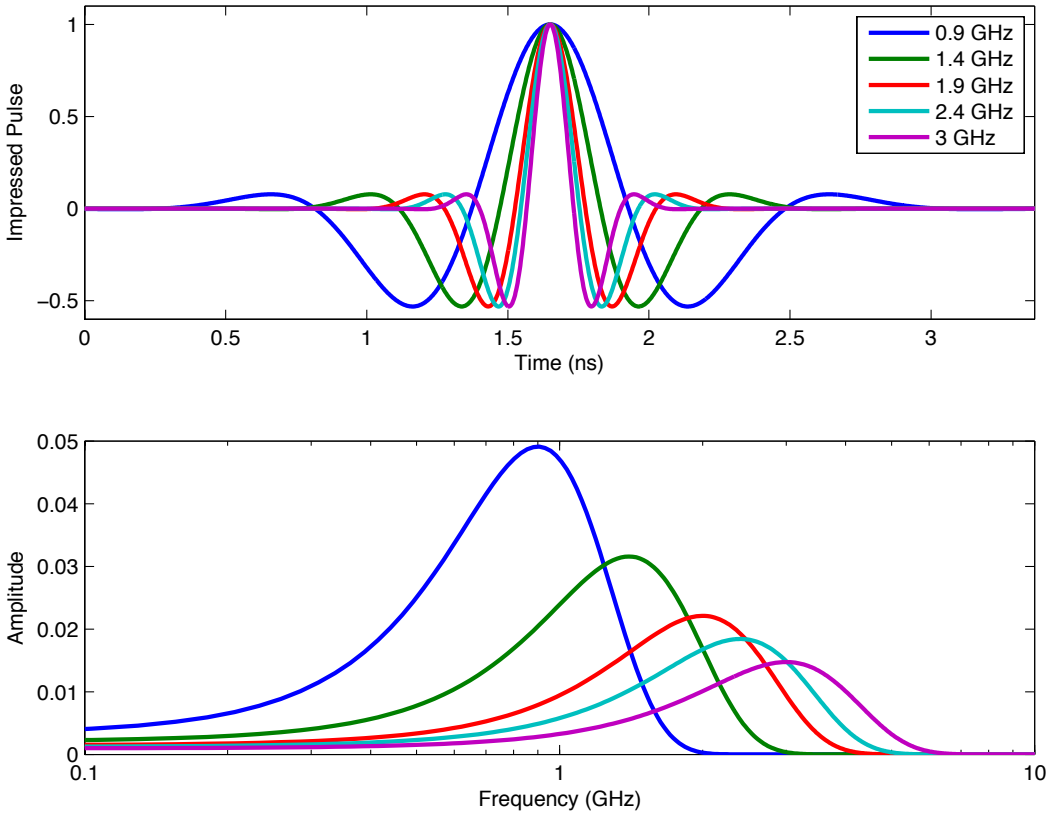

Figure 3: Gaussian-modulated sinusoidal pulses using different central frequencies (11). The fractional bandwidth is constant and equals to $bw = 0.9$.

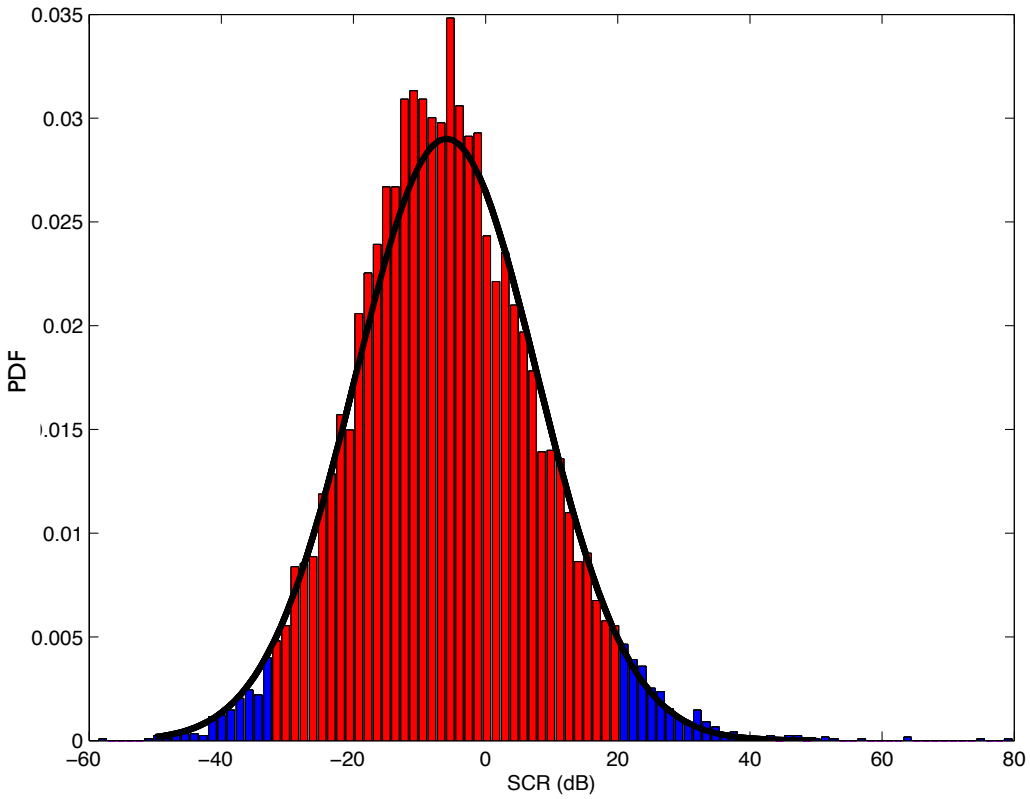

Figure 4: The resulting PDF of SCR using the procedure described in section II.5. Red colour illustrates the values that lie within two standard deviations either side of the mean (-5.9 dB).

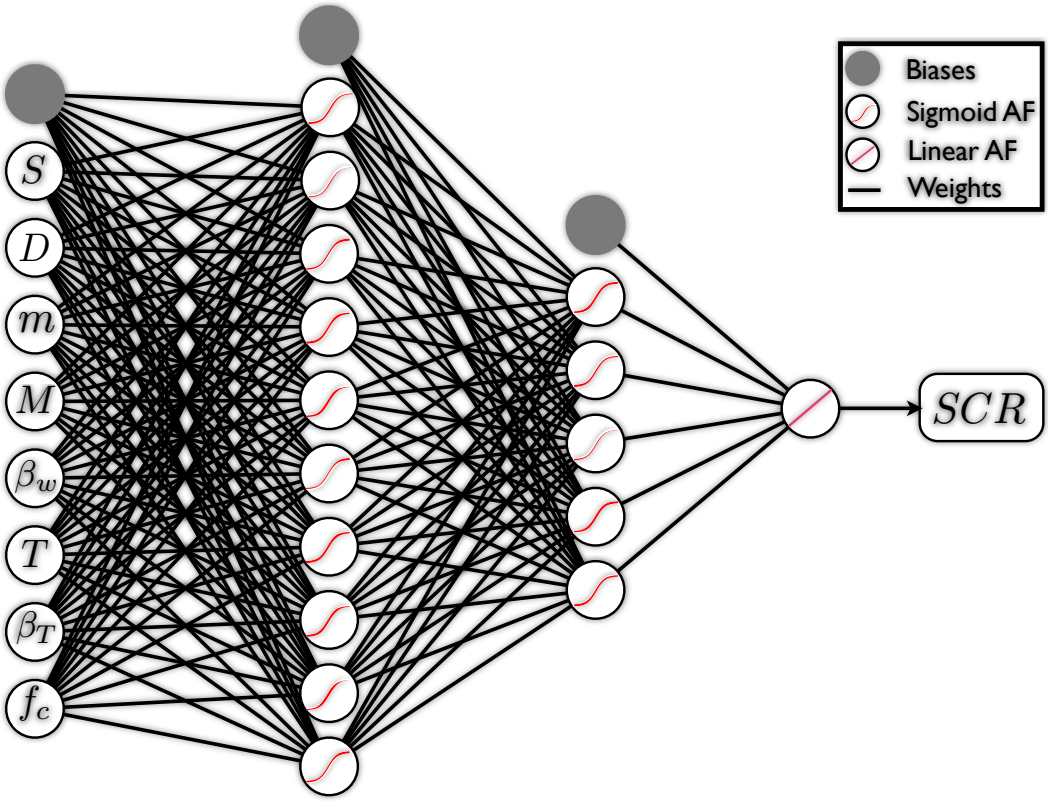

Figure 5: A feedforward ANN is used in an effort to model SCR. The proposed scheme is consisted of two hidden layers with ten and five neurones, respectively.

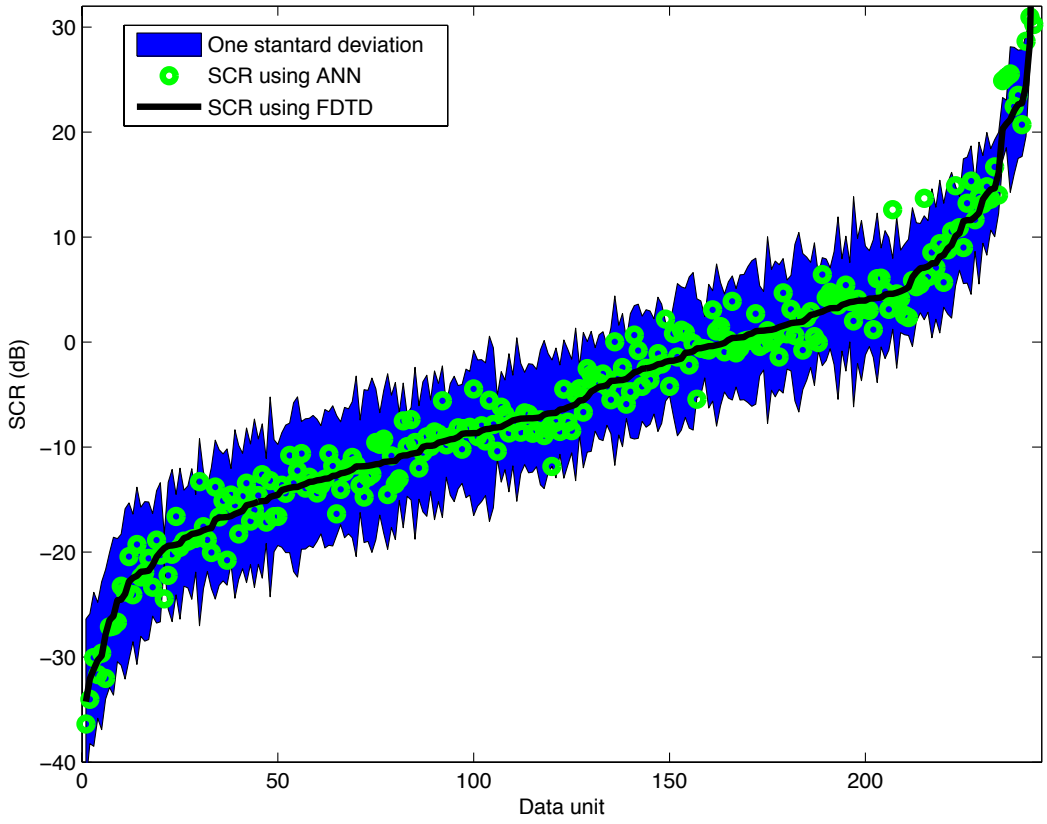

Figure 6: The calculated (using FDTD) and the predicted (using the suggested regression framework) SCR. The blue area represents the range (one standard deviation) of the calculated SCR. The present scenarios are randomly chosen and they are not included into the training set. For illustration purposes the data are plotted with incremental order.

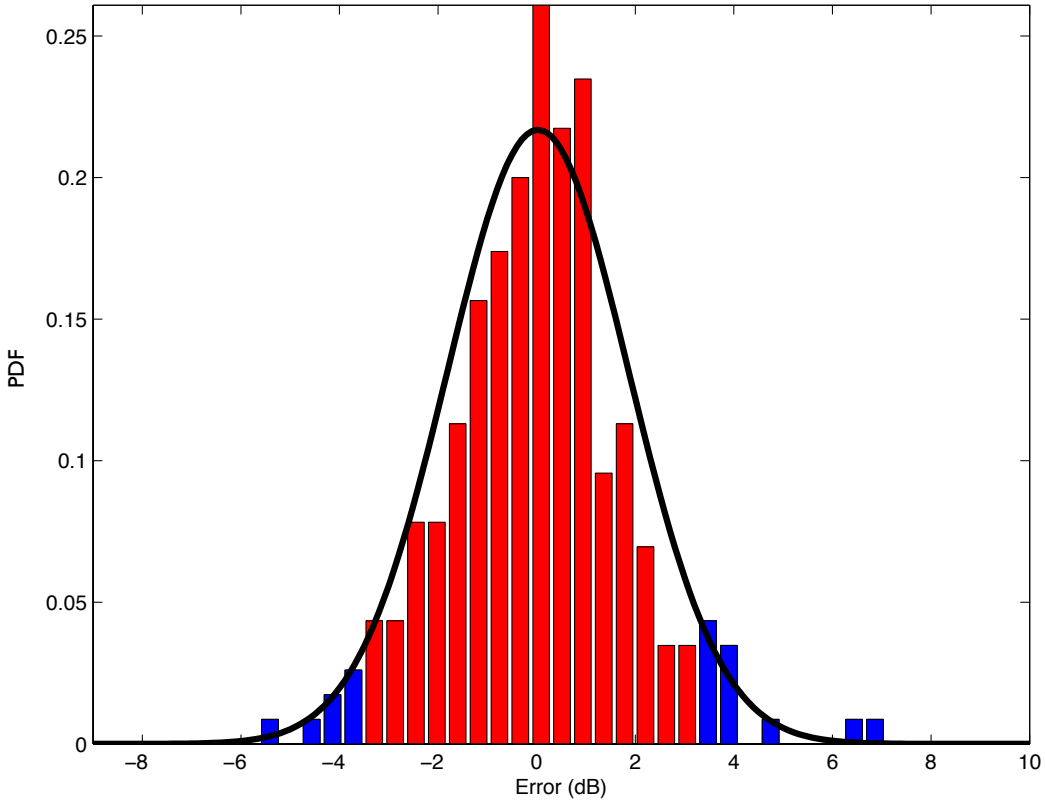

Figure 7: PDF of the error between the calculated (using FDTD) and the estimated (using ANN) SCR. Red colour illustrates the error that lies within two standard deviations either side of the mean.

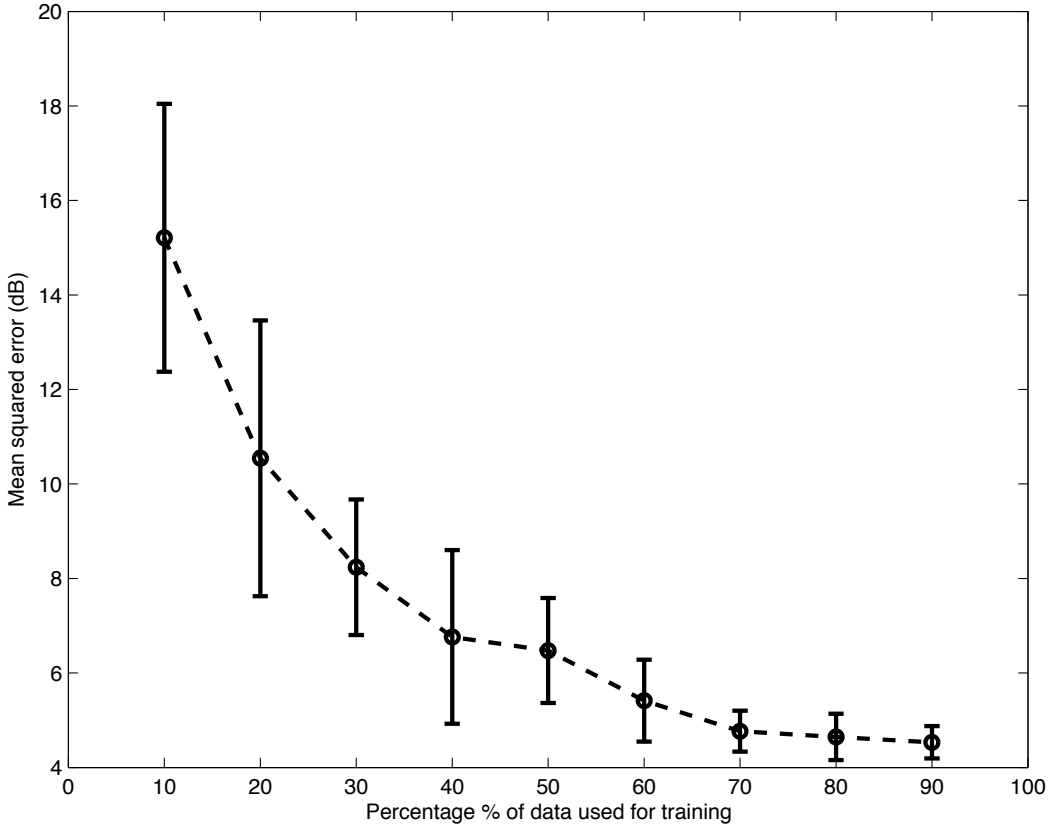

Figure 8: Averaged (over twenty different ANN trained using different initial conditions) mean squared error between the calculated (using FDTD) and the predicted (using ANN) SCR using different percentages of the original database for training and validation purposes. In each case, 10 % of the training set are employed for validation purposes. The error bounds denote one standard deviation of the squared error using different initial weights and biases prior to the training process.

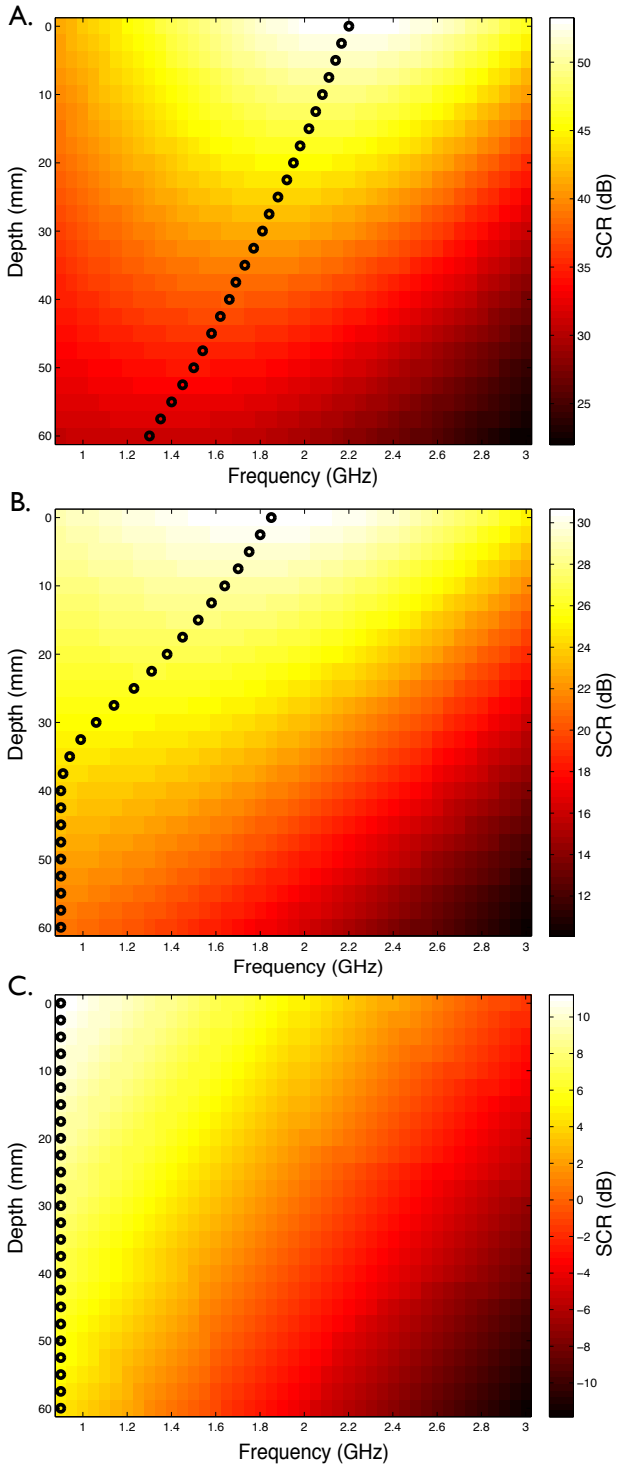

Figure 9: The input parameters are $m = 0.1$, $M = 0.101$, $C = 0.5$, $\beta_T = 3$, $\beta_w = 1$, $f_c = 0.9 - 3$ GHz and $D = 0 - 60$ mm. Three different surface's maximum absolute deviation are considered, A) $T = 0$ mm, B) $T = 2$ mm and C) $T = 20$ mm. Black circles depicts the optimal central frequency with respect to landmine's depth.

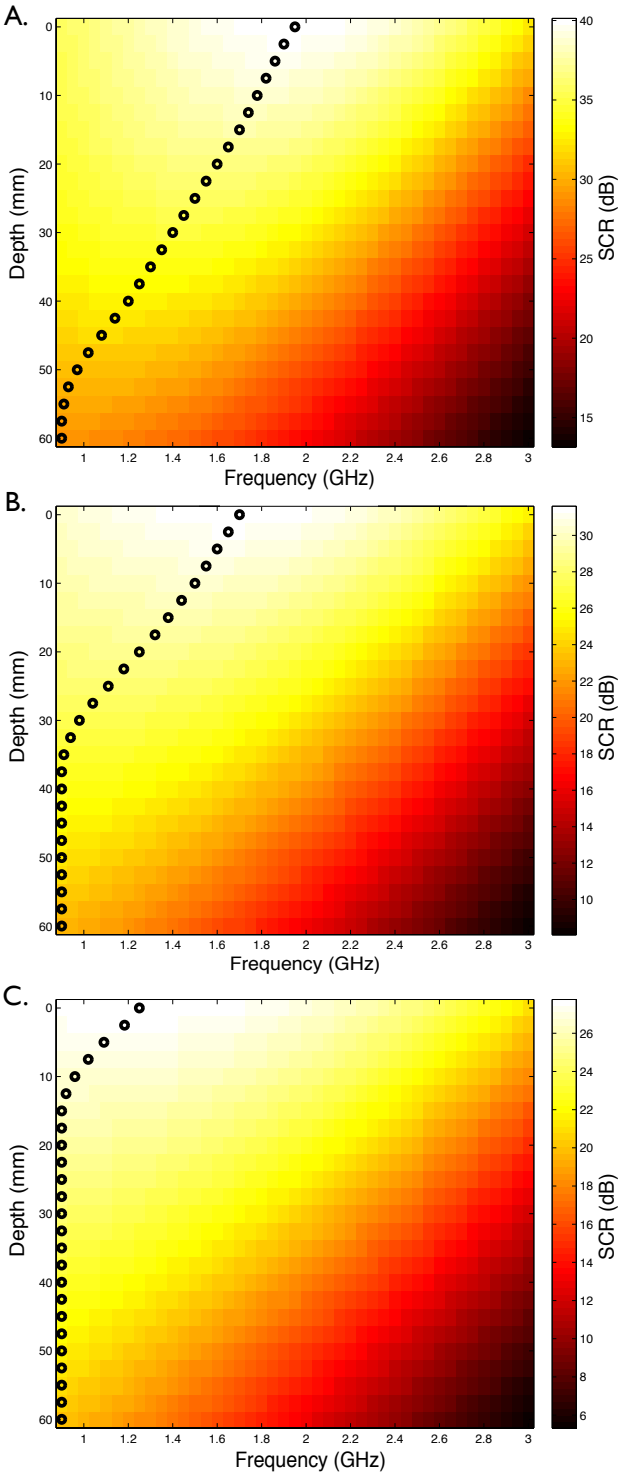

Figure 10: The input parameters are $m = 0.05$, $M = 0.2$, $C = 0.5$, $\beta_T = 3$, $T = 0$, $f_c = 0.9 - 3$ GHz and $D = 0 - 60$ mm. Three different water fraction distributions are examined, A) $\beta_w = 0$, B) $\beta_w = 0.8$ and C) $\beta_w = 1.4$. Black circles depicts the optimal central frequency with respect to landmine's depth.

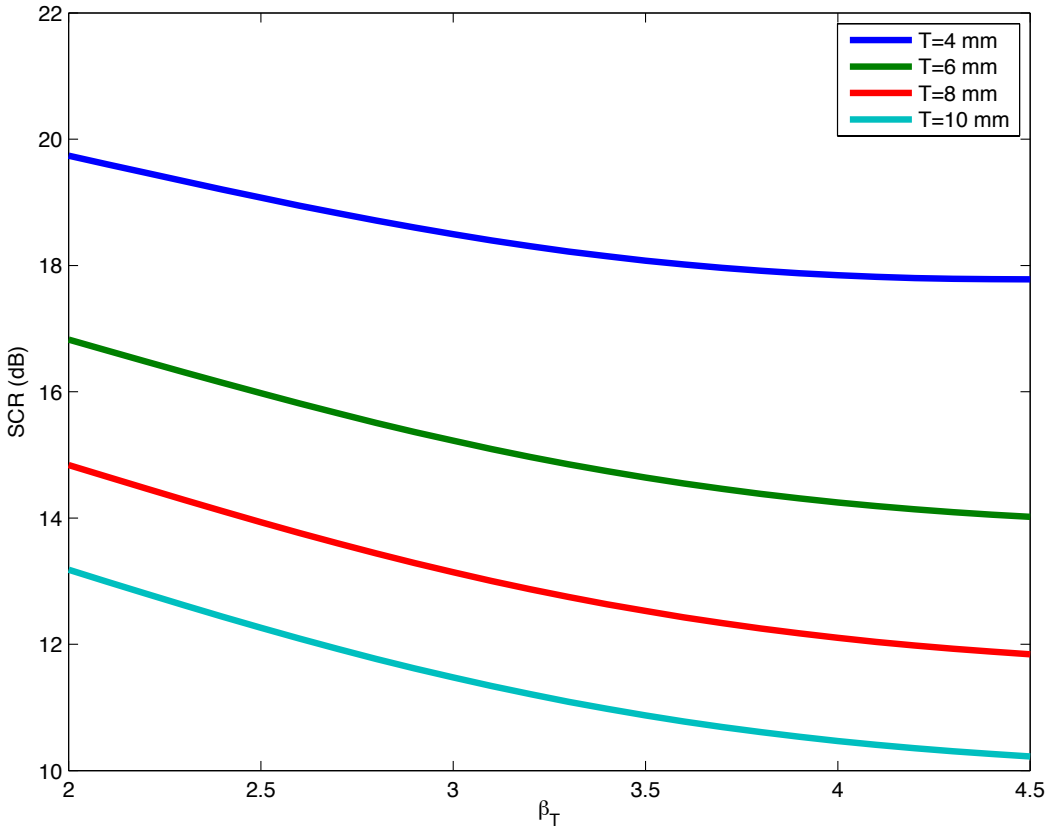

Figure 11: The input parameters are $m = 0.10$, $M = 0.101$, $C = 0.5$, $\beta_w = 1$. $f_c = 1.5$ GHz, $D = 35$ mm, $T = 4 - 10$ and $\beta_T = 2 - 4.5$.

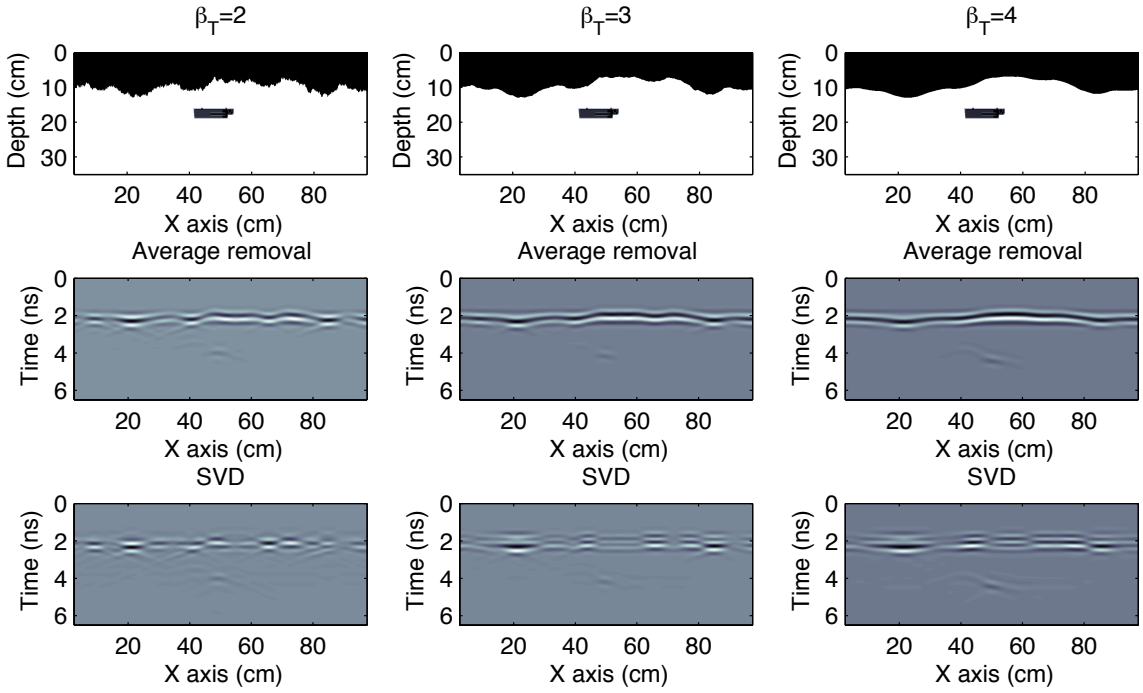

Figure 12: The input parameters are $m = 0.2$, $M = 0.2$, $C = 0.5$, $f_c = 2$ GHz, $D = 40$ mm, $T = 30$ mm and $\beta_T = [2, 3, 4]$. Average removal and SVD (λ_i, $i < 3$) are employed in an effort to remove the direct wave and the ground reflection. Notice that increasing β_T slightly decreases the performance of ground removal techniques as predicted in Fig. 11.